Experimental Mechanics (2019) 59:1223–1232
https://doi.org/10.1007/s11340-019-00531-1

3D Printed Loading Device for Inducing Cellular Mechanotransduction via Matrix Deformation

S.L. Truesdell[1] · E.L. George[1] · C.E. Seno[1] · M.M. Saunders[1]

Received: 20 December 2018 / Accepted: 14 June 2019 / Published online: 1 August 2019

Abstract

This manuscript details the design, fabrication, characterization, and application of a 3D printed loading device for the investigation of cellular mechanotransduction pathways activated by matrix deformation. The device, which works as a screw jack, applies out-of-plane substrate distention to a thin polymer membrane via platen displacement. Load induces a strain gradient on the top surface of the membrane where cells are cultured. A high performance poly-lactic acid 3D filament was used for printing, resulting in a compact, cost-effective device that is fully autoclavable and compatible with standard laboratory incubators. The device was customized to accommodate a loadable polydimethylsiloxane chip developed in our lab for culturing MLO-Y4 osteocytes; however, the design can be easily adapted to load any mechanosensitive cells grown on an elastomeric membrane. Using finite element analysis, we demonstrated that the device can generate a range of strains to induce a variety of responses by the osteocytes. Cell viability data demonstrated that these ranges had the ability to engender load-induced apoptotic differences.

Keywords Mechanotransduction · Matrix deformation · Osteocytes · Finite element analysis · 3D printing

Introduction

Within the body, cells are routinely exposed to a variety of mechanical forces that affect cell proliferation, differentiation, organization, and gene expression. To function properly, many cells require physical anchoring to the extracellular matrix (ECM) via transmembrane glycoproteins, known as integrins [1]. These proteins link the ECM to the cytoskeleton and play a vital role in cellular pathways that translate deformations within the matrix into biochemical signals [2]. The matrix-integrin-cytoskeleton pathway provides a route for rapid signal transduction from the ECM to the cell nucleus, which can ultimately result in alterations in gene expression [3, 4]. Over the past few decades, significant progress has been made in understanding the signaling pathways that regulate cellular mechanotransduction; however, many of the intricacies are yet to be fully realized.

Like many tissues, bone is sensitive to its mechanical environment and can adapt its structure in response to changes in mechanical stimuli. This process, known as bone remodeling, is controlled by mechanosensitive osteocytes. Osteocytes express a variety of surface proteins that are activated by mechanical stretch, including integrins, connexins, and ion channels [5, 6]. Within the bone matrix, osteocyte cell bodies are confined to small cavities called lacunae, and an average of 50-60 dendritic processes per cell extended outward to connect with neighboring cells via gap junctions [7, 8]. Formation of these channels is critical for intracellular signal transduction, and evidence suggests that mechanical stimulation can enhance this communication [9]. Studies have also shown that stretching the cellular membrane opens ion channels, which leads to the activation of calcium-dependent pathways within the cell [10, 11].

Mechanical stimulation induces a number of signaling cascades in osteocytes that occur over a wide temporal range. For example, within seconds of load application, intracellular calcium concentrations are increased and adenosine triphosphate is released from the cell [12, 13]. Within minutes of load application, osteocytes release nitric oxide and increase production of prostaglandin E2 [13, 14]. Following 3 h of stimulation, elevated mRNA expression of several bone proteins, COX-2, osteocalcin, and IGF-1, has been observed [15]. Inaba et al. [16] found that 96 h of loading resulted in significant alterations in cell morphology and an increase in autophagy-related gene expression.

Electronic supplementary material The online version of this article (https://doi.org/10.1007/s11340-019-00531-1) contains supplementary material, which is available to authorized users.

✉ S. L. Truesdell
slt79@zips.uakron.edu

[1] Department of Biomedical Engineering, The University of Akron, 302 E Buchtel Ave, Akron, OH 44325-0302, USA

Additionally, evidence suggests that osteocytes have a biphasic response to the magnitude of the applied load. While moderate loading levels have been shown to prevent osteocyte apoptosis, pathologic loads, such as those seen in fracture, can cause the reverse effect [9, 17]. Substrate stretching that induces damage can disrupt dendritic processes and cause osteocyte cell bodies to separate from the ECM [18–20].

To investigate the mechanisms governing mechanotransduction in bone, our lab has previously developed platforms that subject cells to mechanical stimulation [21, 22]. In York et al. [22], a microactuator was used to apply static, out-of-plane distention to osteocytes seeded on an elastomeric membrane. While the device was useful for stimulating cells short-term on the benchtop, it was not conducive to long-term studies that require cells to be maintained in an incubated environment. The commercial actuator used in this device was controlled with electronic circuitry, and the high humidity within a laboratory incubator could result in a build-up of condensation that would destroy these components. Moreover, the expense of the actuator made production of additional units cost-prohibitive.

As such, we sought to develop a cost-effective loading machine capable of applying similar static loads that could also withstand autoclaving and long-term incubation. The device, which works like a screw jack, was 3D printed using a high performance poly-lactic acid (PLA) filament. We customized the device to accommodate a loadable polydimethylsiloxane (PDMS) chip previously developed in our lab for culturing MLO-Y4 osteocytes [23]. However, the design can be adapted for use with any elastomeric substrate. Finite element analysis (FEA) demonstrated that the device can generate a range of strains to induce a variety of responses by the osteocytes. Cell viability data indicated that these ranges were able to engender apoptotic differences.

Materials and methods

Loading device

The loading device was designed in SolidWorks 2017 (Dassault Systèmes), and an exploded view is shown in Fig. 1. Part files for all 3D printed components (lid, chip holder, base, platen, dial block, and dial) are provided in Online Resources 1, 2, 3, 4, 5, 6. Components were printed with a MakerGear M2 printer using a Raptor Series PLA high performance 3D filament (Maker Geeks). A 1-kg spool (~$35) was sufficient for printing more than two complete sets of parts. After printing, components were annealed for 15 min at 98 °C (30 min ramp time). The manufacturer recommended annealing components for 15 min at 100 °C; however, we found that a slight decrease in temperature, along with the reported ramp time, significantly decreased the likelihood of parts warping during this process while still providing the desired increase in strength and temperature resistance.

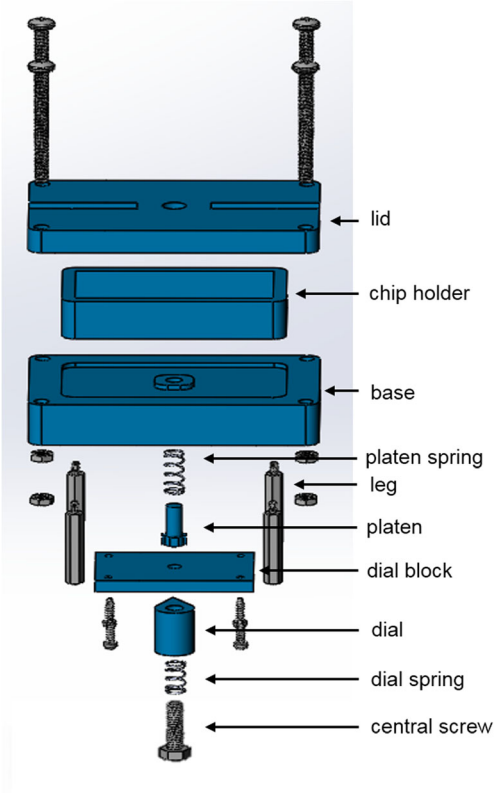

Fig. 1 Exploded view of the loading device design. All printed parts (lid, chip holder, base, platen, dial block, and dial) are shown in blue; commercial hardware is shown in gray

The device was fitted with stainless steel hardware to resist rust formation during autoclaving and incubation cycles. All hardware was purchased from McMaster-Carr for approximately $60. The lid was attached to the base with four M5 × 0.8 mm pan head screws (50 mm long, 92000A340) and thin hex nuts (90710A037). Clearance holes, which were oversized by 0.2 mm to compensate for material expansion during the annealing process, were incorporated into the printed designs for the lid and base. Four M3 × 0.5 mm male-female threaded hex standoffs (6 mm hex size, 31 mm long, 93655A722) served as legs. Drill holes for the legs were incorporated into the bottom of the base design, and the holes were manually tapped after printing and annealing. The dial block was attached to the bottom of the base with four M3 self-tapping screws for thin plastic (10 mm long, 96817A910). Clearance holes, oversized by 0.2 mm, were incorporated into the dial block, and drill holes were incorporated into the bottom of the base. An additional drill hole was incorporated in the center of the dial block design; after printing and annealing, the hole was manually tapped to accommodate the central screw. An M6 × 1 mm hex head screw (20 mm long, 93635A212) was selected for the central screw, which controls the vertical displacement of the platen. The dial aided in

rotating the central screw during loading and contained a hexagonal-shaped hole that fit over the head of the central screw. A clearance hole was incorporated in the top of the dial to allow the shaft of the central screw to move vertically. Both of these holes were again oversized by 0.2 mm. A compression spring (12.7 mm long, 7.62 mm OD, 6.5 mm ID, 9002 T16) was used to apply force to the top of the dial to keep it firmly pressed against the dial block. The diameter of the dial spring was selected to fit loosely around the shaft of the central screw while still allowing the head of the screw to serve as a stop for the lower end of the spring. The lengths of the central screw and dial spring were selected such that at a neutral loading position, the spring maintained a slight compressive preload to maintain force on the dial. The spring was short enough when fully compressed to allow the central screw to be displaced up to 9 mm. This created a wide range of possible loading displacements. A platen spring (1.75 mm long, 7.62 mm OD, 6.5 mm ID, 9002 T23) was selected to loosely fit around the shaft of the platen and generate force on the bottom lip of the platen to return it to the original position as load was removed.

Performance characterization

To validate the performance of the device, vertical platen displacements were verified. Slack was removed from the system by lowering the platen below the zero mark before bringing it back up to zero. The dial was then rotated to the theoretical platen displacement of 1 or 2 mm. The device was photographed from the side (Fig. 2). Gauge blocks (1.5875 mm and 2.5400 mm) were placed directly next to the platen to serve as reference lengths. Actual vertical displacements of the platen were then measured using ImageJ [24]. For each sample the displacement was measured along each side of the platen and averaged. This process was repeated nine times for each displacement.

PDMS fabrication

A PDMS chip for loading MLO-Y4 osteocytes was developed by our lab (Fig. 3a). The design, fabrication, and sterilization procedures have been previously described [23]. Briefly, the chip consists of a PDMS well, 10 mm deep and 9 mm in diameter. The bottom of the well was formed by a 0.5 mm-thick PDMS membrane (Fig. 3b). During loading, this membrane was tented from below by the platen (Fig. 3c). A previous study in our lab demonstrated that a thickness of at least 0.5 mm was required to ensure the membrane would not rupture during the loading process [25]. The chip was sealed with a 3 mm thick PDMS lid. PDMS used for the chip and the lid was made by combining Sylgard® 184 polymer base and curing agent in a 10:1 ratio; it was cured overnight at 45 °C.

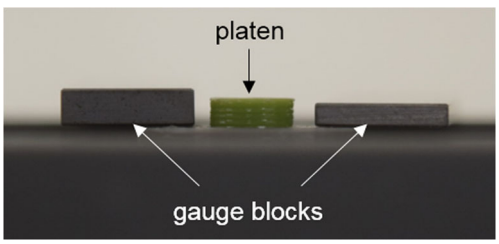

Fig. 2 Representative image of a 2 mm platen displacement. Gauge blocks served as reference lengths of 2.5400 mm (left) and 1.5875 mm (right)

Finite element analysis

A static non-linear finite element analysis (FEA) was used to estimate the substrate strains generated on the surface of a PDMS membrane when tented from below with the circular platen. MLO-Y4 osteocytes seeded on the top surface of the membrane were subjected to strains generated by the PDMS deformation during a 15-min loading period. A static model was chosen due to the significant time difference between the platen translation (a few seconds) and the load application (15 min).

The FEA model was developed using SolidWorks Simulation 2017. *Version 1.1* of the model consisted of the entire PDMS chip bonded to the platen component of the loading device (Fig. 4a). In *Version 2.1*, the model was refined to remove areas of the PDMS chip and platen that had no effect on the simulation outcome. The chip was reduced to a 15-mm diameter cylinder centered on the well, and the height of the chip was reduced to 5.5 mm (Fig. 4b). Fillets with a 0.1-mm radius were added around the base of the well and the top of the platen to decrease the effect of singularities on the results. The platen was also reduced to a 2-mm-thick cylinder. The model was further simplified by taking radial symmetry into account, with *Version 2.2* representing a 90° sector of *Version 2.1* (Fig. 4c).

The PDMS was modeled as a nonlinear, incompressible, hyperelastic material. A two-parameter Mooney-Rivlin hyperelastic model was used [26, 27]:

$$W = c_1(I_1-3) + c_2(I_2-3)$$

where W represents the strain energy function, $c_1$and c_2 are empirically determined material parameters, and I_1 and I_2 are the first and second invariants of the left Cauchy-Green deformation tensor. The PDMS material parameters c_1 and c_2 depend on the ratio of polymer base to curing agent. Experimental parameters were obtained from literature for a 10:1 ratio and are shown in Table 1 [28].

The platen was modeled as a linear, elastic, isotropic material. Material properties for PDMS and PLA were obtained from literature and are summarized in Table 2 [29, 30].

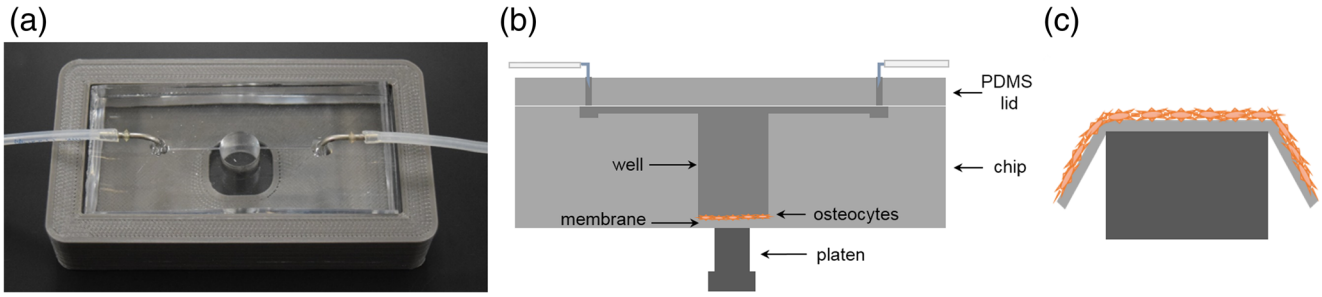

Fig. 3 **(a)** Image of a PDMS chip that was sealed with a lid and placed within the chip holder. Tubing used for cell seeding and feeding was connected to the chip via access holes punched through the lid, **(b)** Schematic side view of the sealed chip seeded with osteocytes. When the chip is placed within the loading device, the platen is aligned beneath the membrane as shown, **(c)** During bouts of loading the platen translates upward to tent the membrane from below as shown

A solid curvature-based mesh was applied to the entire system. The maximum and minimum element sizes were 1.38 mm and 0.276 mm, respectively. A mesh convergence study was performed by applying a mesh refinement to the top and bottom surfaces of the PDMS membrane (Fig. 4d). The maximum element size on these surfaces was decreased in 50 μm increments from 600 μm to 250 μm.

A prescribed displacement was applied to the outer cylindrical surface of the platen; the motion was restricted to the upward vertical direction. The platen was concentrically aligned with the PDMS well, and the top surface of the PDMS chip was fixed by setting all translational degrees of freedom to zero. Symmetry boundary conditions were applied to surfaces on the orthogonal planes that reduced the model to a 90° sector. Simulations were completed at six platen displacements: 1.0, 1.2, 1.4, 1.6, 1.8, and 2.0 mm. The average and maximum equivalent strains and von Mises stresses at the top surface of the PDMS membrane were determined for each displacement using the surface probe tool. This feature restricted the strain outputs to values exclusively at the top surface of the membrane. The equivalent strain (ε_e) was computed as:

$$\varepsilon_e = \frac{1}{1+\nu}\sqrt{\frac{(\varepsilon_1-\varepsilon_2)^2+(\varepsilon_2-\varepsilon_3)^2+(\varepsilon_3-\varepsilon_1)^2}{2}}$$

where ν represents Poisson's ratio and ε_1, ε_2, and ε_3 represent the normal principal strains [31]. The von Mises stress or equivalent stress ($\sigma_{e)}$ was computed as:

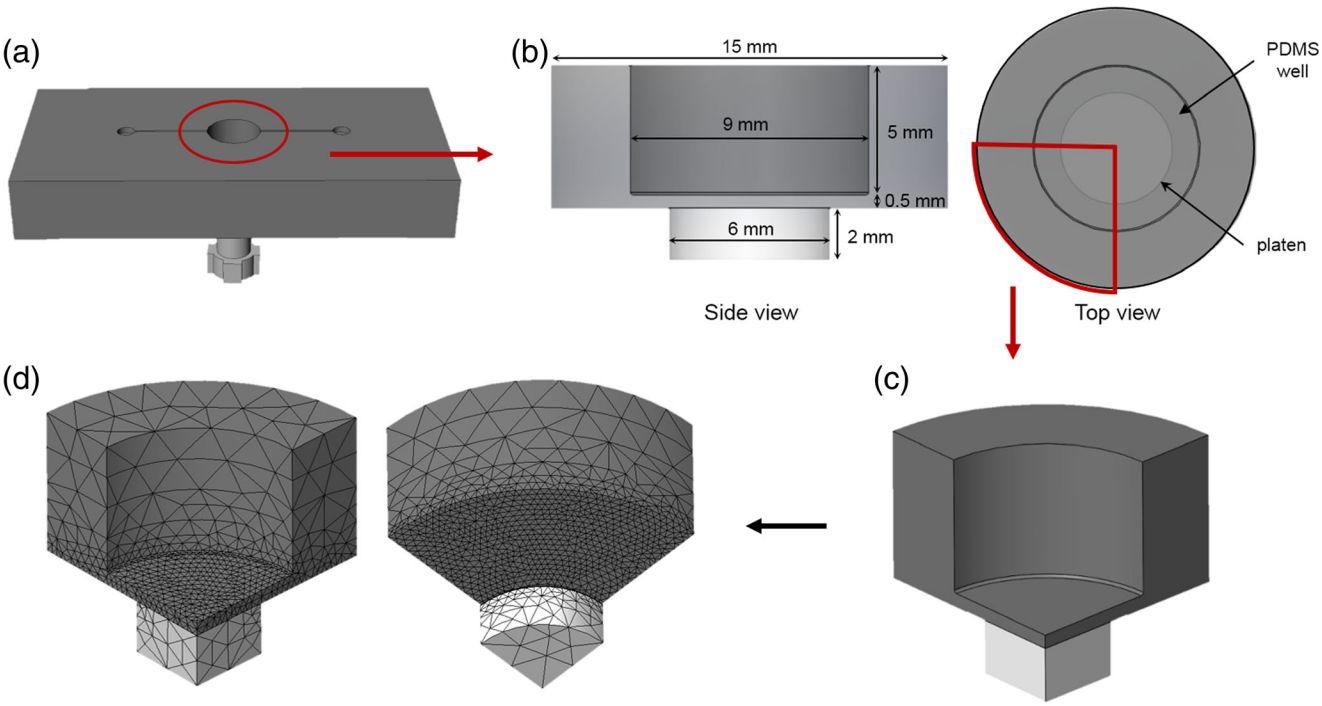

Fig. 4 (**a**) Version 1.1 incorporating the full chip and platen, (**b**) side and top view of Version 2.1 consisting of a 15-mm diameter section of the PDMS chip around the well and a 2-mm-high section of the platen, (**c**) Version 2.2 representing a 90° sector of Version 2.1, (**d**) Top and bottom view of Version 2.2 after mesh refinement was applied to both sides of the PDMS membrane with an element size of 250 μm

Table 1 Mooney-Rivlin parameters

Parameter	Value (MPa)
c_1	0.237
c_2	0.06

$$\sigma_e = \sqrt{\frac{(\sigma_1-\sigma_2)^2 + (\sigma_2-\sigma_3)^2 + (\sigma_3-\sigma_1)^2}{2}}$$

where σ_1, σ_2, and σ_3 represent the normal principal stresses [31].

Osteocyte cell culture

MLO-Y4 osteocytes (a generous gift from Dr. Lynda Bonewald) were seeded into the type-I-collagen (CTI)-coated chips at a density of 20,000 cells/ml in minimum essential alpha medium (Gibco) supplemented with 5% calf serum (Hyclone), 5% fetal bovine serum (Hyclone), and 1% penicillin/streptomycin (Sigma) and maintained at 5% CO_2 and 37 °C. After 72 h, medium was replaced. At 96 h, cells were exposed to 15 min of out-of-plane substrate distention using the 3D printed loading device followed by a 90-min post-load incubation period, during which the platen was returned to the original position. Cells were maintained at 5% CO_2 and 37 °C throughout the load and post-load periods.

Flow cytometry

Following loading and incubation, cell culture medium was discarded and 150 μl 0.25% Trypsin-EDTA (Gibco) was added to each well. Cells were incubated for 3 min at 37 °C and 5% CO_2 and 300 μl fresh culture medium was added. Cell suspensions were mixed thoroughly and removed from PDMS wells. Cell staining for the Muse™ Annexin V & Dead Cell assay was performed in the dark and according to manufacturer's instructions. Briefly, 100 μl of each suspension was mixed with 100 μl Muse™ Annexin V & Dead Cell Reagent. Cells were stained for 20 min. Samples were assessed and partitioned into four populations (quadrants) using the Muse™ Cell Analyzer. The following information was determined: concentrations of viable cells, cells in the early stages of apoptosis, cells in the late stages of apoptosis or that have undergone apoptosis, and necrotic cells. Due to the small sample size ($n = 5$) statistical analysis was not conducted.

Table 2 Material properties for PDMS and PLA

Material property	PDMS	PLA
Poisson's ratio	0.49	0.36
Mass density (kg/m^3)	965	1252
Tensile strength (MPa)	5.13	59
Yield strength (MPa)		70
Elastic modulus (MPa)		3500

Results

Loading device

The loading device was printed using a high performance PLA 3D filament. Dimensions for the lid, base, platen, dial, and dial block are shown in Fig. S1a-f. During loading, the lid of the loading device (Fig. S1a) was connected to the base with four stainless steel screws and thin hex nuts to hold the chip in place above the platen. The device was customized to accommodate a loadable PDMS chip previously developed in our lab [23]. A rectangular chip holder was designed to house the chip and minimize the application of preload on the cells (Fig. S1b). The chip holder also improved the accuracy of centering the PDMS well directly above the platen, as the holder fit into indentations on the top surface of the base and the bottom surface of the lid. The central hole in the bottom of the base (Fig. S1c) and the base of the platen (Fig. S1d) were designed to comprise a lock and key system. The blocks protruding from the base of the platen fit into grooves in the base to prevent the platen from rotating during loading. Thus, movement of the platen was restricted to the vertical direction and the possibility of applying unintended torque to the cells by twisting the substrate was eliminated. The top 2-mm space within the hole of the base was designed with a circular opening. This allowed the cylindrical shaft of the platen to pass through but served as a stop for the platen spring. The small ledge at the base of the platen served as a stop for the opposite end of the spring. During loading, the compressed spring generated a downward force on the platen, which pushed the platen back down to the original position as load was removed. A similar design was used for the dial, which was fabricated with a hexagonal-shaped hole to fit over the head of the central screw (Fig. S1e). The top 2-mm space within the hole was designed with a circular opening that allowed the shaft of the central screw to pass through but served as a stop for the dial spring. The head of the central screw served as the second stop for the spring. The spring generated an upward force on the dial to keep it uniformly pressed against the dial block (Fig. S1f). Four stainless steel male-female threaded hex standoffs were attached to the bottom of the base to serve as legs and provide clearance for the dial. The fully assembled device can be seen in Fig. 5a.

Mechanical load was applied to cells seeded within the PDMS chip by rotating the dial, which created equal rotation of the central screw. This resulted in vertical displacement of the central screw through a tapped screw hole located in the

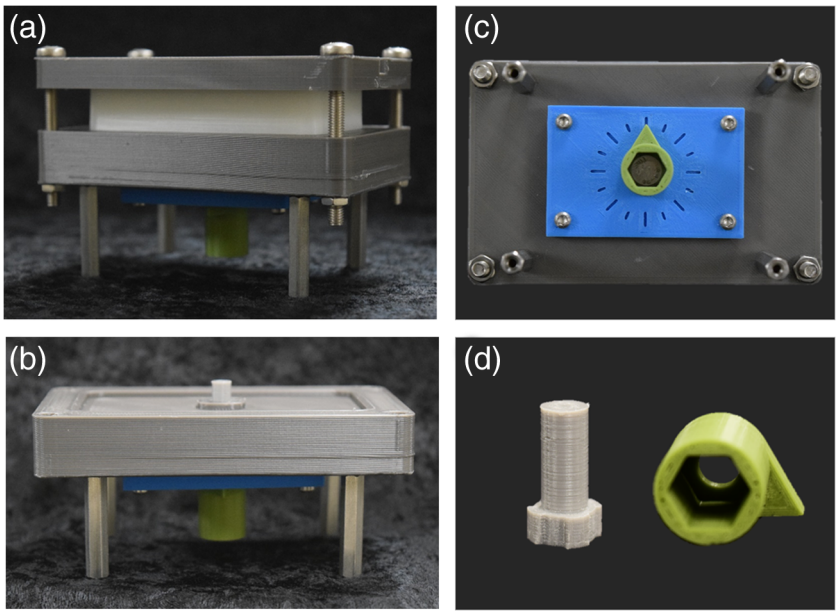

Fig. 5 3D printed loading device(**a**) fully assembled device, (**b**) image of platen moving up through the base to tent membrane, (**c**) bottom view of the device showing incremental tick marks that improve accuracy of partial dial rotations, (**d**) close-up view of platen (left) and dial (right)

center of the dial plate. As the central screw moved upward, it pushed on the bottom surface of the platen and caused the top of the platen to move up out of the base (Fig. 5b). The top surface of the platen pushed against the thin membrane of the PDMS chip located within the chip holder. The vertical displacement per rotation of the dial was controlled by the thread pitch of the central screw. The device was designed such that one full rotation of the dial resulted in a 1-mm vertical displacement of the platen. The dial block incorporated incremental tick marks around the hole for the central screw that allowed for a higher degree of accuracy with partial dial rotations (Fig. 5c). Close-up images of the printed platen and dial are shown in Fig. 5d. After printing, components were annealed, which increased the strength and heat resistance of the material. As a result, the material could withstand multiple autoclaving cycles (30 min, 121 °C) without any obvious signs of warping.

Performance characterization

The performance of the device was analyzed by measuring the vertical displacement of the platen after applying dial displacements of 1 and 2 mm. For each displacement, the device was tested nine times. For a 1-mm displacement, the average vertical displacement of the platen was 0.99 mm ± 0.006 mm (mean ± standard errors of the means). For a displacement of 2 mm, the average vertical displacement of the platen was 1.99 mm ± 0.01 mm (mean ± standard errors of the means).

Finite element analysis

The loading device described here can be used to apply a strain to a PDMS membrane. This study focused only on the strain gradient generated on the top surface of the membrane; the cells were cultured on this surface. Loading was modeled using six vertical displacements between 1 mm and 2 mm. At each displacement, mesh convergence analysis was performed by decreasing the mesh element size on the top and bottom surfaces of the PDMS membrane. Mesh convergence was evaluated by comparing the total number of elements to the average equivalent strain (Fig. 6a) and average von Mises stress (Fig. 6b) generated on the top surface of the PDMS membrane.

It was determined that an element size of 250 μm was sufficient to ensure that the output was independent of the mesh geometry. This mesh sizing corresponds to approximately 11,900 elements within the entire model. For all displacements, the peak strain and peak stress on the top surface of the membrane were generated just above the outer ring of the platen and decreased radially in both directions. Color maps of the strain and stress distributions are shown for 1-mm and 2-mm displacements (Fig. 6c,d).

The average, maximum, and minimum equivalent strains and von Mises stresses produced on the top surface of the PDMS membrane at each of the six vertical displacements are shown in Table 3. With a vertical platen displacement between 1 mm and 2 mm, the average surface strain on the PDMS membrane is between 8.56% and 16.59% and the average stress is between 178 and 318 kPa.

Osteocyte viability

MLO-Y4 osteocytes seeded on the CTI-coated PDMS membrane (Fig. 7a) were loaded with platen displacements of 0 mm (no load), 1 mm, or 2 mm. The Muse™ Annexin V

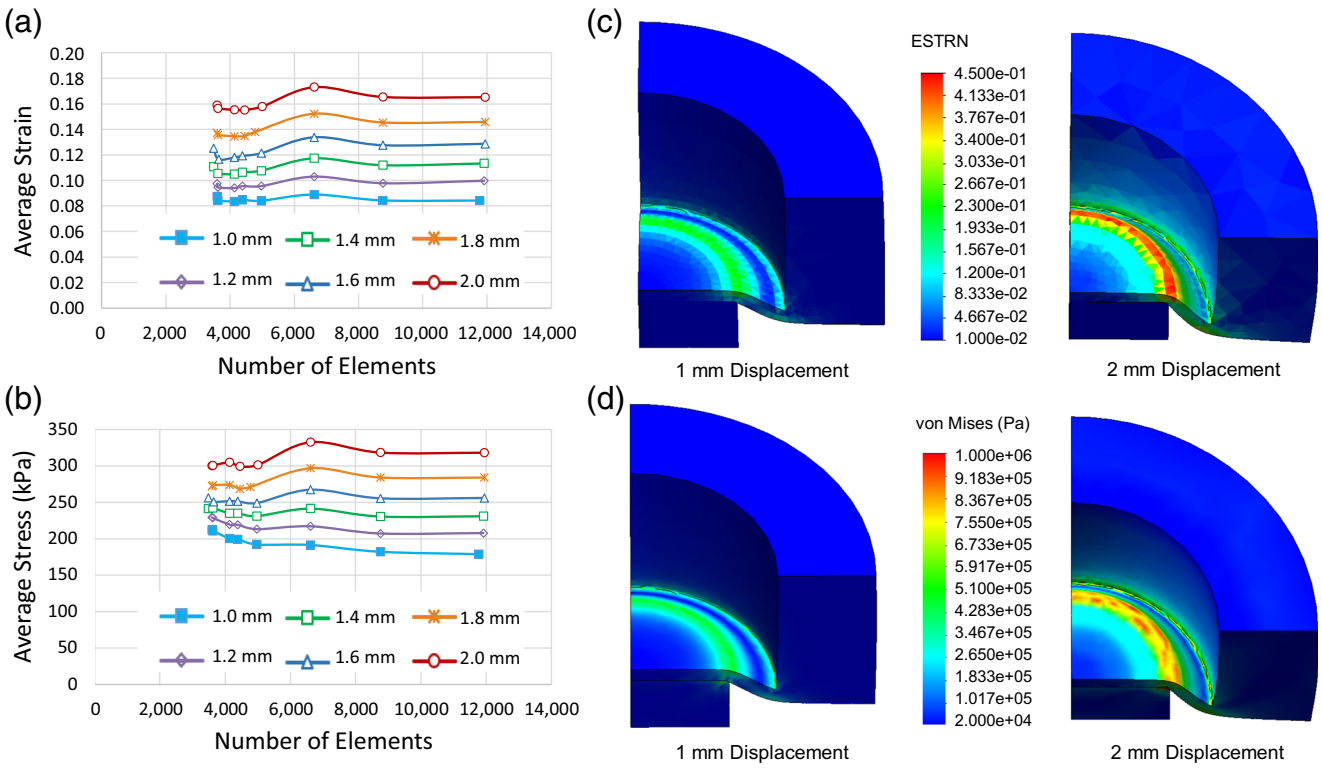

Fig. 6 Mesh convergence results for (**a**) the average equivalent strain (ESTRN) and, (**b**) the average von Mises stress generated on the top surface of the PDMS membrane. Color maps of the (**c**) strain distribution and (**d**) stress distribution on the top surface of PDMS membrane resulting from platen displacement of 1 and 2 mm

& Dead Cell assay was used to categorize cells into four distinct populations: live, early apoptotic, late apoptotic or those that have undergone apoptosis, and dead necrotic cells. A small sample ($n = 5$) of chips were loaded to demonstrate that osteocytes are sensitive to strains generated in this range. Results of the Muse™ Annexin V & Dead Cell assay are shown in Fig. 7b. These data establish an emerging trend that suggests an increase in vertical displacement (surface strain) may be positively correlated with an increase in the percentage of apoptotic cells. Representative results for the four populations at each loading condition are shown in Fig. 7c.

Discussion

The goal of this work was to create a simple, cost-effective loading device that could be easily fabricated and customized by researchers in a variety of fields with a range of technical backgrounds. The device described here applies static, out-of-plane distention via platen displacement to cells cultured on a PDMS membrane. This type of load can be used to stimulate cellular mechanotransduction pathways through deformation of the ECM. A screw jack design was used to generate platen displacement, which reduced the number of movable parts and resulted in a portable standalone device.

Table 3 Equivalent strain and von Mises stress generated on PDMS surface at six platen displacements

Displacement (mm)	Average Strain	Maximum Strain	Minimum Strain	Average Stress (kPa)	Maximum Stress (kPa)	Minimum Stress (kPa)
1.0	0.08464	0.2325	0.01075	178.2	506.0	19.43
1.2	0.1002	0.2758	0.01283	207.0	618.3	20.53
1.4	0.1139	0.3187	0.01488	230.3	722.9	6.856
1.6	0.1292	0.3591	0.01691	255.3	824.9	20.22
1.8	0.1463	0.4030	0.01873	283.5	924.2	30.00
2.0	0.1659	0.4465	0.02045	317.7	1021	32.77

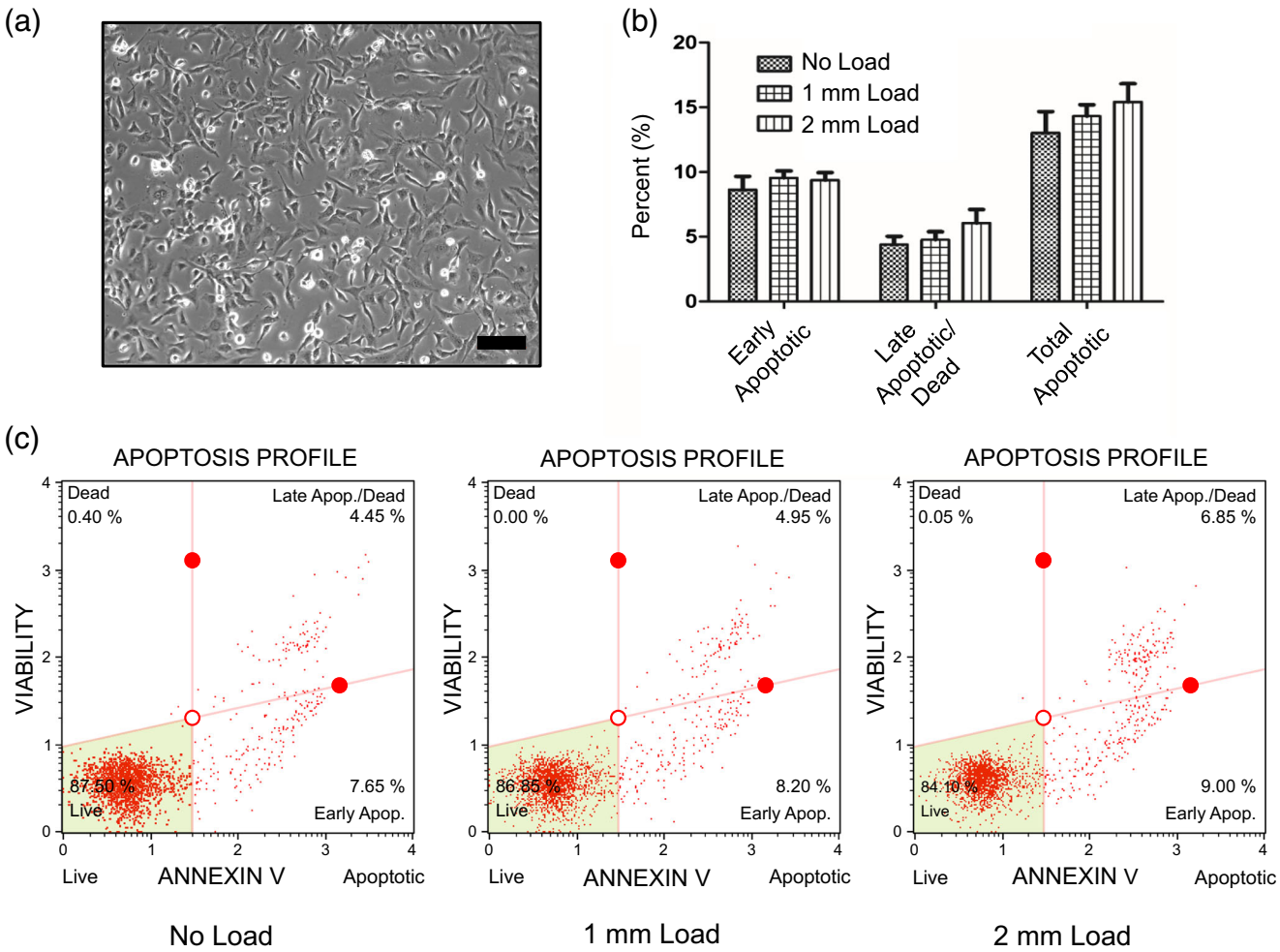

Fig. 7 (**a**) MLO-Y4 osteocytes in the PDMS chip at 96 hrs. Scale bar represents 100 μm, (**b**) Load-induced apoptosis as indicated by the Annexin V & Dead Cell assay. Error bars represent the standard errors of the means, (**c**) Representative viability results at three platen displacements

We used 3D printing to fabricate the device – this offered several advantages. Compared to conventional machining techniques that require skilled operators, 3D printing offers a significantly less expensive method. In fact, our device was fabricated for less than $100. In recent years, the cost of 3D printers has significantly decreased, making the technique widely available. However, 3D printing does not achieve the tight tolerances produced by traditional machining. Therefore, we characterized the performance of the device and found the vertical platen displacement to be within 1% of the theoretical value. Given that this error translates to a much lower error in the strain generated on the membrane, we regarded it as acceptable. Another of our goals was to ensure that the device was compatible with standard sterilization and incubation protocols. Conventional filaments used for 3D printing are composed of plastic materials unable to withstand the high heat and humidity present during autoclaving and incubation. However, following annealing, the Raptor Series PLA used for our device was able to withstand multiple autoclaving and incubation cycles without warping. If damage does occur, replacement parts can be reprinted on demand and multiple units can be rapidly produced for large studies.

We intend to use this device with a PDMS chip previously developed in our lab [23]. However, the device allows for a high degree of flexibility and can be easily adapted to meet user specifications. For example, the chip holder can be replaced with a new design such as the one shown in Fig. S2, to make the device compatible with the use of any elastomeric membrane. Additionally, the range of induced surface strains can be easily adjusted. We modeled strains generated on a 0.5-mm thick PDMS membrane using platen displacements between 1 and 2 mm. With the current design, platen displacements between 0 and 9 mm can be applied. To apply different strains or increase the sensitivity of the device, the type, thickness, or composition of the polymer can be adjusted. The sensitivity can also be increased by using a central screw with a smaller thread pitch.

To demonstrate the applicability of the device we applied load to MLO-Y4 osteocytes. However, it should be noted that the goal was not to provide a thorough investigation of the osteocytic response to matrix deformation, but merely to show that the device can induce a detectable difference in cellular activity. We chose to model transient pathologic overload. Osteocyte mechantransduction pathways can be induced by a variety of mechanical stimuli, though evidence suggests that pathologic bone remodeling is dominated by matrix deformations acting directly on the cells [6, 32–34]. Pathologic conditions such as fracture can result in strain magnitudes of 5% or more [34]. However, studies have shown that the ECM and pericellular matrix can amplify applied strains by more than a factor of three at the cellular level [33, 35, 36]. Thus, we used FEA to model platen displacements that resulted in average strains in the neighborhood of 15%. To examine the cellular response to the applied strains, we analyzed cell viability. Evidence suggests that mechanotransduction from pathologic loads is triggered by an increase in osteocyte apoptosis at the damage site [18]. Our results were consistent with this evidence and show an emerging trend that suggests an increase in average surface strain is positively correlated with an increase in apoptotic/dead cells. In addition, it is possible that a longer load time or a longer post-load incubation would produce a more significant difference in apoptotic response.

Conclusions

To stimulate mechanotransduction by matrix deformation, we created a 3D printed loading device capable of applying static, out-of-plane distention to cells on a PDMS membrane. The standalone device is cost-effective, fully autoclavable, and compatible with standard laboratory incubators. Additionally, the device can be easily customized to accommodate cells on any elastomeric membrane. Using FEA, we showed that the device can generate a range of strains on the membrane surface to model a variety of pathologic conditions. Finally, we demonstrated that our system is sensitive enough to promote load-induced apoptotic differences in MLO-Y4 osteocytes.

Acknowledgements The authors would like to thank Mr. Stephen Paterson for his help with 3D printing. This work was supported by the National Science Foundation under Grant Nos. (CBET 1060990 and EBMS 1700299). Also, this material is based upon work supported by the National Science Foundation Graduate Research Fellowship Program under Grant No. (2018250692). Any opinion, findings, and conclusions or recommendations expressed in this material are those of the authors and do not necessarily reflect the views of the National Science Foundation.

References

1. Wang N (2017) Review of cellular mechanotransduction. J Phys D Appl Phys 50(23):233002
2. Wittkowske C, Reilly GC, Lacroix D, Perrault CM (2016) *In vitro* bone cell models: Impact of fluid shear stress on bone formation. Front Bioeng Biotechnol 4:87. https://doi.org/10.3389/fbioe.2016.00087
3. Duncan RL, Turner CH (1995) Mechanotransduction and the functional response of bone to mechanical strain. Calcif Tissue Int 57(5):344–358. https://doi.org/10.1007/bf00302070
4. Gusmão CVBD, Belangero WD (2009) How do bone cells sense mechanical loading? Rev Bras Ortop 44(4):299–305. https://doi.org/10.1016/S2255-4971(15)30157-9
5. Feng X, McDonald JM (2011) Disorders of bone remodeling. Annu Rev Pathol 6:121–145. https://doi.org/10.1146/annurev-pathol-011110-130203
6. Klein-Nulend J, Bacabac RG, Bakker AD (2012) Mechanical loading and how it affects bone cells: the role of the osteocyte cytoskeleton in maintaining our skeleton. Eur Cell Mater 24:278–291
7. Hemmatian H, Bakker AD, Klein-Nulend J, van Lenthe GH (2017) Aging, osteocytes, and mechanotransduction. Curr Osteoporos Rep 15(5):401–411. https://doi.org/10.1007/s11914-017-0402-z
8. Klein-Nulend J, Bakker AD, Bacabac RG, Vatsa A, Weinbaum S (2013) Mechanosensation and transduction in osteocytes. Bone 54(2):182–190. https://doi.org/10.1016/j.bone.2012.10.013
9. Plotkin LI, Bellido T (2013) Beyond gap junctions: Connexin43 and bone cell signaling. Bone 52(1):157–166. https://doi.org/10.1016/j.bone.2012.09.030
10. Wang Y, McNamara LM, Schaffler MB, Weinbaum S (2007) A model for the role of integrins in flow induced mechanotransduction in osteocytes. Proc Natl Acad Sci U S A 104(40):15941–15946. https://doi.org/10.1073/pnas.0707246104
11. Mikuni-Takagaki YJJB, Metabolism M (1999) Mechanical responses and signal transduction pathways in stretched osteocytes. J Bone Miner Metab 17(1):57–60. https://doi.org/10.1007/s007740050065
12. Lewis KJ, Frikha-Benayed D, Louie J, Stephen S, Spray DC, Thi MM, Seref-Ferlengez Z, Majeska RJ, Weinbaum S, Schaffler MB (2017) Osteocyte calcium signals encode strain magnitude and loading frequency *in vivo*. Proc Natl Acad Sci U S A 114(44):11775–11780. https://doi.org/10.1073/pnas.1707863114
13. Robling AG, Turner CH (2009) Mechanical signaling for bone modeling and remodeling. Crit Rev Eukaryot Gene Expr 19(4):319–338
14. Rawlinson SCF, Pitsillides AA, Lanyon LE (1996) Involvement of different ion channels in osteoblasts' and osteocytes' early responses to mechanical strain. Bone 19(6):609–614. https://doi.org/10.1016/S8756-3282(96)00260-8
15. Kawata A, Mikuni-Takagaki Y (1998) Mechanotransduction in stretched osteocytes–temporal expression of immediate early and other genes. Biochem Biophys Res Commun 246(2):404–408. https://doi.org/10.1006/bbrc.1998.8632
16. Inaba N, Kuroshima S, Uto Y, Sasaki M, Sawase T (2017) Cyclic mechanical stretch contributes to network development of osteocyte-like cells with morphological change and autophagy promotion but without preferential cell alignment in rat. Biochem Biophys Rep 11:191–197. https://doi.org/10.1016/j.bbrep.2017.04.018
17. Tan SD, Bakker AD, Semeins CM, Kuijpers-Jagtman AM, Klein-Nulend J (2008) Inhibition of osteocyte apoptosis by fluid flow is mediated by nitric oxide. Biochem Biophys Res Commun 369(4):1150–1154. https://doi.org/10.1016/j.bbrc.2008.03.007
18. Jilka RL, Noble B, Weinstein RS (2013) Osteocyte apoptosis. Bone 54(2):264–271. https://doi.org/10.1016/j.bone.2012.11.038

19. Yavropoulou MP, Yovos JG The molecular basis of bone mechanotransduction. J Musculoskelet Neuronal Interact 16(3): 221–236
20. Noble BS, Peet N, Stevens HY, Brabbs A, Mosley JR, Reilly GC, Reeve J, Skerry TM, Lanyon LE (2003) Mechanical loading: biphasic osteocyte survival and targeting of osteoclasts for bone destruction in rat cortical bone. Am J Physiol Cell Physiol 284(4): C934–C943. https://doi.org/10.1152/ajpcell.00234.2002
21. King JD, York SL, Saunders MM (2016) Design, fabrication and characterization of a pure uniaxial microloading system for biologic testing. Med Eng Phys 38(4):411–416. https://doi.org/10.1016/j.medengphy.2016.01.011
22. York SL, King JD, Pietros AS, Newby BZ, Sethu P (2015) Saunders MM Development of a microloading platform for *in vitro* mechanotransduction studies. In, Cham. *Mechanics of Biological Systems and Materials, Volume 7*. Springer International Publishing, pp 53-59
23. George EL, Truesdell SL, York SL, Saunders MM (2018) Lab-on-a-chip platforms for quantification of multicellular interactions in bone remodeling. Exp Cell Res 365(1):106–118. https://doi.org/10.1016/j.yexcr.2018.02.027
24. Schindelin J, Arganda-Carreras I, Frise E, Kaynig V, Longair M, Pietzsch T, Preibisch S, Rueden C, Saalfeld S, Schmid B, Tinevez J-Y, White DJ, Hartenstein V, Eliceiri K, Tomancak P, Cardona A (2012) Fiji: an open-source platform for biological-image analysis. Nat Methods 9:676. doi:https://doi.org/10.1038/nmeth.2019 https://www.nature.com/articles/nmeth.2019#supplementary-information
25. Shah KS, York SL, Sethu P, Saunders MM (2013) Developing a microloading platform for applications in mechanotransduction research. In: Prorok BC, Barthelat F, Korach CS et al. (eds) *Mechanics of Biological Systems and Materials, Volume 5*, New York, NY, 2013//. Springer New York, pp 197-205
26. Mooney M (1940) A theory of large elastic deformation. J Appl Phys 11(9):582–592. https://doi.org/10.1063/1.1712836
27. Rivlin RS (1948) Large elastic deformations of isotropic materials. IV. Further developments of the general theory. Philos Trans A Math Phys Eng Sci 241(835):379–397
28. Paul BK, Abhinkar BS, Lee S (2011) High pressure hermetic compression seals for embedding elastomeric membrane microvalves in polymer microfluidic devices. Precis Eng 35(2):348–354. https://doi.org/10.1016/j.precisioneng.2010.09.008
29. Farah S, Anderson DG, Langer R (2016) Physical and mechanical properties of PLA, and their functions in widespread applications — A comprehensive review. Adv Drug Deliv Rev 107:367–392. https://doi.org/10.1016/j.addr.2016.06.012
30. Johnston ID, McCluskey DK, Tan CKL, Tracey MC (2014) Mechanical characterization of bulk Sylgard 184 for microfluidics and microengineering. J Micromech Microeng 24(3):035017
31. Petrova RV (2014) Introduction to Static Analysis Using SolidWorks Simulation. CRC Press, Hoboken
32. Bonewald LF (2011) The amazing osteocyte. J Bone Miner Res 26(2):229–238. https://doi.org/10.1002/jbmr.320
33. Bonivtch AR, Bonewald LF, Nicolella DP (2007) Tissue strain amplification at the osteocyte lacuna: A microstructural finite element analysis. J Biomech 40(10):2199–2206. https://doi.org/10.1016/j.jbiomech.2006.10.040
34. You J, Yellowley CE, Donahue HJ, Zhang Y, Chen Q, Jacobs CR (2000) Substrate deformation levels associated with routine physical activity are less stimulatory to bone cells relative to loading-induced oscillatory fluid flow. J Biomech Eng 122(4):387–393
35. Verbruggen SW, Vaughan TJ, McNamara LM (2012) Strain amplification in bone mechanobiology: a computational investigation of the *in vivo* mechanics of osteocytes. J R Soc Interface 9(75):2735–2744. https://doi.org/10.1098/rsif.2012.0286
36. Wang L, Dong J, Xian CJ (2015) Strain amplification analysis of an osteocyte under static and cyclic loading: A finite element study. Biomed Res Int 2015:14. https://doi.org/10.1155/2015/376474